

Artificial intelligence and quasar absorption system modelling; application to fundamental constants at high redshift

Chung-Chi Lee¹★, John K. Webb²†, R. F. Carswell³, and Dinko Milaković⁴.

¹*DAMTP, Centre for Mathematical Sciences, University of Cambridge, Cambridge CB3 0WA, UK*

²*School of Physics, University of New South Wales Sydney, NSW 2052, Australia*

³*Institute of Astronomy, Madingley Road, Cambridge CB3 0HA, UK*

⁴*European Southern Observatory, Karl-Schwarzschild-Str. 2, 85748 Garching bei München, Germany*

Accepted XXX. Received YYY; in original form ZZZ

ABSTRACT

Exploring the possibility that fundamental constants of Nature might vary temporally or spatially constitutes one of the key science drivers for the European Southern Observatory’s ESPRESSO spectrograph on the VLT and for the HIRES spectrograph on the ELT. High-resolution spectra of quasar absorption systems permit accurate measurements of fundamental constants out to high redshifts. The quality of new data demands completely objective and reproducible methods. We have developed a new fully automated Artificial Intelligence-based method capable of deriving optimal models of even the most complex absorption systems known. The AI structure is built around VPFIT, a well-developed and extensively-tested non-linear least-squares code. The new method forms a sophisticated parallelised system, eliminating human decision-making and hence bias. Here we describe the workings of such a system and apply it to synthetic spectra, in doing so establishing methods of importance for future analyses of VLT and ELT data. The results show that modelling line broadening for high-redshift absorption components should include both thermal and turbulent components. Failing to do so means it is easy to derive the wrong model and hence incorrect parameter estimates. We also argue that model non-uniqueness can be significant, such that it is not feasible to expect to derive an unambiguous estimate of the fine structure constant α from one or a small number of measurements. No matter how optimal the modelling method, it is a fundamental requirement to use a large sample of measurements to meaningfully constrain temporal or spatial α variation.

Key words: Cosmology: cosmological parameters; Methods: data analysis, numerical, statistical; Techniques: spectroscopic; Quasars: absorption lines; Line: profiles; Abundances

1 INTRODUCTION

The development of optimal, objective, and reproducible methods for the analysis of high-resolution absorption systems is essential for analysing the high quality data now being obtained on new astronomical facilities. Forthcoming facilities like the ELT clearly demand sophisticated analytic tools. Searches for new physics, revealed by temporal or spatial variations in fundamental constants, constitute one of the three main science drivers for the ESPRESSO spectrograph on the European Southern Observatory’s VLT (Pepe et al. 2014), and one of the key goals for the forthcoming ELT (Hook 2009; ESO ELT team 2010, 2011; Liske et al. 2014; Marconi et al. 2016).

Bainbridge & Webb (2017a,b) first developed AI methods that were capable of modelling arbitrarily complex absorption systems without any human interactions. At the heart of the process is VPFIT (Carswell & Webb 2014, 2020), a non-linear least squares system with tied parameter constraints. The additional genetic code acts as a wrapper, guiding the descent direction to an optimal solution on the basis of a test statistic (the corrected Akaike Information Criterion). Hybrid algorithms of this sort have been coined “memetic” (Moscato 1989).

In the present paper, we develop these ideas further, the key aims being to find faster algorithms and improve the overall performance, particularly for complex absorption systems/datasets that may be challenging to model, comprising a wide range of line strengths, from heavily saturated to barely detected, allowing for any blended absorption lines from other systems.

Performance checking focuses on estimating the fine structure constant in quasar absorption systems, because this is a particularly

★ E-mail: lee.chungchi16@gmail.com

† E-mail: jkw@phys.unsw.edu.au

challenging problem, more so than simple 3-parameter absorption line fitting. Whilst the newly created methods introduced in this paper have been developed in the context of quasar spectroscopy, they are likely to be useful in any absorption line spectroscopy application, including stellar spectroscopy and terrestrial experiments.

In Section 2 we explain the various stages of the AI algorithm, which we call “AI-VPFIT”. We partition the process into 6 stages, describing the design of each in detail. Section 3 evaluates the performance of AI-VPFIT using synthetic spectra. Section 4 shows that it is important to properly model the absorption line width and that not doing has a significant impact on parameter estimation. In Section 5, we discuss how an objective AI method removes biases inherent to previous interactive analyses and show that model non-uniqueness limits the accuracy achievable from a single measurement of variation in the fine structure constant $\Delta\alpha/\alpha$. Extensive use is made of the corrected Akaike Information Criterion for comparing the relative improvement in model development at each stage. The pros and cons of this are discussed in Section 6. Finally, in Section 7 we summarise AI-VPFIT’s key characteristics and performance, the main findings from extensive testing using synthetic data, and the implications and requirements of future measurements to constrain $\Delta\alpha/\alpha$ using quasar spectroscopy.

2 THE AI METHOD

The new algorithms described in this paper follow the broad principles outlined in Bainbridge & Webb (2017a,b) although there are notable differences and many new algorithms. These include: (i) as described in the following text, trial line positions are random; (ii) the ordering of the various tasks carried out here is different here compared to Bainbridge & Webb (2017a,b); (iii) Bayesian model averaging is not used here; we next describe each stage of the modelling process; (iv) GVPFIT was set up to use either fully turbulent or fully thermal broadening. This turns out to be a significant issue (discussed in detail later in this paper). The new method presented here does not make these assumptions; (v) two new stages are included to refine the model and address the overfitting problem.

2.1 Stage 1 – Creating a preliminary model using a primary species or primary transitions

In general, the combined dataset will be comprised of multiple spectral segments, to be fitted simultaneously. In Stage 1, partially for computing speed considerations, we first build a preliminary model prior to modelling the entire dataset. The choice of the *primary reference transition* (or *transitions*) or a *primary reference species* is important.

A simple example might be fitting an absorption system comprised of multiple FeII transitions and the MgII 2796/2803 doublet. Let us assume, in this example, that all transitions fall longwards of the Lyman- α forest. If this is a damped Lyman- α system in which both MgII lines are mostly saturated, the sensible primary species choice is FeII.

On the other hand, for a non-DLA system, with generally lower column densities, the MgII lines may be strong but unsaturated and the FeII features may be sufficiently weak that some velocity components seen in MgII are below the detection threshold in FeII. In this case, the MgII absorption complex provides the better constraint on velocity structure and may be more suited as the primary species.

To give further examples, the requirement may be to use a single species, e.g. FeII to solve for the fine structure constant α ,

or many ^2H lines to solve for the electron to proton mass ratio μ . In these cases, the *primary transition* (or transitions) are selected to be the data segment (or segments) that are likely to provide the most reliable initial model. To clarify, consider the following example. Suppose we have two FeII transitions, 1608 and 2383Å, the former falling in the Lyman- α forest (and hence being blended with HI lines at various redshifts), the latter falling longwards of the Lyman- α emission line. In this situation, the FeII 2383Å line should be treated as the *primary* transition and the FeII 1608Å line as the secondary transition.

The fine structure constant α (and/or if fitting molecular lines, the electron to proton mass ratio μ) may be included as a free parameter in this Stage. However, this can only be done if the primary species or primary transitions are comprised of 2 or more transitions with sufficiently different sensitivities to α variation so as to avoid degeneracy with redshift z . It is important to include these parameters from the outset, rather than first deriving a best-fit model for the entire dataset and *only then* adding those free parameters, since this would inevitably bias α (or μ towards the terrestrial value).

Having decided on the species to be used as the *primary species*, Monte Carlo methods are used to construct the model, simultaneously for all primary species’ transitions. Initially, a single model absorption line is placed at random within the complex. Its absorption line parameters (N and b) are default initial values, always the same, user-defined and provided by an input parameter file.

The algorithm above thus provides an initial first-guess model for the primary species. Non-linear least-squares, VPFIT, (Carswell & Webb 2014, 2020), is used to refine the initial parameters. At this point (initial iteration), we are likely to have a very poor fit to the data, using only a single profile to model an arbitrarily complex dataset. The goodness-of-fit is quantified using the corrected Akaike Information Criterion (AICc),

$$AICc = \chi_p^2 + \frac{2nk}{n - k - 1}, \quad (1)$$

where n and k are the numbers of data points and model parameters, respectively, and

$$\chi_p^2 = \sum_{i=1}^n \frac{(F_{i,data} - F_{i,model})^2}{\sigma_i^2} \quad (2)$$

where $F_{i,data}$, $F_{i,model}$, and σ_i are the observed spectral flux, the model fit, and the estimated error on $F_{i,model}$ for the i^{th} pixel and the subscript p indicates a summation for the primary data only.

As is well known, the second term in Eq. (1) penalises χ^2 , to prevent an arbitrarily large number of free parameters being introduced. Other statistics such as the Bayesian Information Criterion (BIC) perform a similar function but impose a stronger penalty. We defer a comparison between the various options to a forthcoming paper.

At the end of this process (Generation 1) We now have the best-fit single-profile model and can thus begin to refine the model i.e. increase its complexity until we have a statistically acceptable representation of the data. This best-fit 3-parameter model thus now becomes the parent for Generation 2, in which a second trial line is placed randomly in redshift z within the fitting range¹, assigning the trial line the same initial default parameters as before. Non-linear least-squares refinement is again carried out and AICc computed. If

¹ In practice, the range is defined by the lowest and highest redshift available over the multiple data segments used.

AICc has decreased compared to Generation 1, the current model is accepted as the Generation 2 best-fit, becoming the parent for the next generation. If AICc has *increased* compared to Generation 1, the model is rejected, the process repeated (i.e. a second trial line is used, again randomly placed in redshift), until AICc decreases. We call each iteration of this procedure one generation.

Iterating the above gradually increases the model complexity and improves the fit. The loop is terminated only after no reduction in AICc can be found after a user-defined number of trials (parameter N_{line} , set in the same initialisation file).

2.2 Stage 2 – Include secondary species

Stage 1 results in a good fit to the primary species alone (MgII in our example). Stage 2 comprises two steps. Firstly, the overall dataset being fitted is increased by adding in all secondary species (FeII in our example). The absorption system structure derived in Stage 1, i.e. the best-fit set of redshifts, is replicated for each secondary species to be fitted. The initial model for the secondary species is relatively crude in that each redshift component for each of the secondary species is assigned default trial values of the column density N . The velocity dispersion parameters b can be related either by the limiting cases of entirely “thermal” broadening ($b_s = b_p \sqrt{m_p/m_s}$), where the subscripts p and s refer to primary and secondary species), entirely “turbulent” broadening ($b_s = b_p$), or in-between (i.e. the gas temperature T is included as a free parameter). This is discussed in detail in Section 2.7). Then, non-linear least-squares refines the parameters for all secondary species, after which AICc is again computed and stored.

If solving for either α or μ , and if this free parameter was not introduced in Stage 1 (see earlier discussion), it can be included at this Stage. Including α (or μ) *prior* to developing a complete model is important to avoid bias.

The second step within Stage 2 is to increase the model complexity, i.e. further redshift components are added, one at a time, until no descent in AICc can be found for N_{line} trials. Once this happens, the Stage 2 model is complete.

2.3 Stage 3 – Adding interlopers

So far, we have assumed that no unidentified absorption lines are present anywhere in the data. This is generally not the case. Each quasar sightline typically intersects multiple distinct absorption systems, such that blending between lines arising in different redshift systems is common.

There are two types of interlopers: (i) an absorption system at some other known redshift. In this case the interloper species and rest-wavelength may be identified and there may be other transitions in the same ion or from other ions at the same redshift that can be modelled simultaneously in order to best constrain the interloper parameters, or (ii) the interloper species/origin is unknown. If the interloper is identified beforehand as being of type (i), then the overall model to be fitted can include the appropriate free parameters from the outset, that is, the set-up prior to Stage 1 indicates that 2 redshift systems are to be simultaneously fitted.

If we have an interloper of type (ii), all previous (non-interloper) line parameters from Stages 1 and 2 are initially (here, in Stage 3) *fixed*. The reason for doing this is as follows. χ^2 minimisation will act so as to ‘prefer’ the interloper (since the interloper has no tied parameters, unlike the heavy element line) such that the interloper may tend to replace the heavy element line. Physically, this is obviously incorrect.

To identify possible interlopers, there are 2 potential procedures: (a) Each data segment is treated separately. An interloper is added in a random position within each data segment, one at a time, and VPFIT allowed to iterate to derive the best-fit interloper parameters (or to reject the interloper entirely), or (b) All data segments are dealt with at the same time i.e. one interloper is placed in each data segment simultaneously, with wavelength

$$\lambda_{interloper}^i = (1 - R) \times \lambda_{min}^i + R \times \lambda_{max}^i \quad (3)$$

where R is the random seed from 0 – 1 and $\lambda_{min(max)}^i$ is the minimum (maximum) wavelength of the i th segment. One could generate a different random seed for each wavelength segment but this offers no advantage.

Superficially, (a) is the favoured option because (b) has a potential systematic trend towards over-fitting the data (i.e. fitting the data with too many absorption components). The reason for this is because introducing one single interloper at a time, and using AICc to check whether that interloper is justified, results in a final model that only contains parameters that are statistically required. On the other hand, introducing one interloper into each segment simultaneously does not permit individual AICc testing on each interloper (because of tied parameters, it is not possible to define AICc on a region-by-region basis). This argument suggests that procedure (a) is preferable in order to avoid over-fitting. However, procedure (a) is computationally very time consuming – e.g. if we have 10 data segments to be fitted, the time required is 10 times as long. In terms of computing time, it is more efficient to adopt procedure (b) and subsequently test for over-fitting and repair the model where necessary (Stage 5).

2.4 Stage 4 – Refine and add new parameters (continuum and zero levels)

This Stage comprises two steps.

Step 1: Firstly, we release all the previously-fixed primary and secondary parameters such that they can be freely varied. Then, additional primary and secondary components are added, one per generation. No new interlopers are included. As before, this process terminates only when no AICc descent occurs within N_{line} trials.

Step 2: At this point we have only considered parameters associated with absorption lines themselves. We have not yet considered additional important parameters, such as the continuum level nor a possible zero level correction. The second step in Stage 4 is therefore to add in these additional parameters (if they are required), and refine the model again using AICc and N_{line} .

2.5 Stage 5 – Mutation; repeat earlier stages

This Stage allows the model to evolve further to allow for the introduction of new continuum and zero-level parameters. By the end of Stage 4, a good model has already been achieved. However, since that model has been derived prior to including continuum and zero-level parameters, several procedures need repeating. Therefore:

- (i) All continuum and zero-level parameters are temporarily fixed;
- (ii) The algorithm is returned to Stage 2, but the Stage 2 starting (i.e. first guess) model parameters are those from the end of Stage 4 (step 2), but all interlopers previously found are removed;
- (iii) Stages 2 to 4 are then repeated. The previously-fixed continuum and zero-level parameters are returned to free parameters are the

(repeated) Stage 4/step 2. The loop is closed by a user-set (or default) AI-VPFIT setting, which defines the number of repeats.

We now explain the reasons behind the 3 processes immediately. If, prior to this stage, the original continuum placement was slightly wrong, then because we may be fitting multiple transitions from a single species (e.g. several FeII transitions), a continuum error may result in a poor fit once secondary transitions are included.

This point can be clarified by example. Suppose our primary species is FeII2383 and one secondary transition is the weaker (lower oscillator strength) FeII2344. Suppose further that the original continuum placement for FeII2344 was placed slightly too low. In this example, it could easily be the case that an interloper (coincident with the FeII2344 position) provides a greater reduction in AICc compared to the (real) FeII2344 line. Such an effect clearly produces problems as follows. The lowest AICc may then be found by reducing the FeII column density so as to achieve a good fit at both lines, but an interloper is placed in the FeII2383 line to compensate for the continuum placement error.

Slight errors in the original continuum placement can also lead to the following problem. If, again, the original continuum had been slightly too low in places, interlopers which in reality are present in the spectrum may have been missed. Repeating Stages 2 and 3 guards against this possibility.

2.6 Stage 6 – Check for over-fitting and refine model parameters further

2.6.1 Preparation

1. Reproduce velocity structure from primary species into all secondary species. Reason: some of the secondary species components could have been dropped. Therefore put all secondary components back but remove all dropping criteria. Setting dropping criteria requires striking a balance between avoiding insignificant parameters in the final model and hence having ill-conditioned matrices yet at the same time avoiding losing relevant parameters. One reason for doing this is that in a system with multiple velocity components, during the iterative sequence, a parameter which is ultimately determined to be important, temporarily falls below a dropping criterion, so could be incorrectly removed. By removing the a dropping criterion, the search direction (and step) can become unstable through ill-conditioning. This would cause difficulties in the absence of a temporary control. Therefore, during this Stage, we place an upper bound on parameter update step sizes.

2. The second action taken at this stage is to fix any continuum and zero level parameters to those best-fit values obtained at the end of Stage 4. This turns out to be helpful for the following reason. Since here, in Stage 5, we re-initialise the secondary species absorption line parameters (either to a set of default values or otherwise), the model is temporarily placed further away from the best-fit solution. The potential consequence of this can be that any sudden increase in (for example) a continuum parameter level can be compensated by a corresponding increase in absorption line strength (i.e. an increase in either N or b or both). In other words, a satisfactory model may sometimes be found corresponding to a local minimum in χ^2 space. This problem is avoided by preventing (temporarily) further adjustment in either the continuum or zero level parameters.

3. The third action taken at this stage is to temporarily fix all redshifts (for both heavy element lines and interlopers). Again, because this Stage temporarily moves the current model away from the final best-fit model, as in point 2 above, the slight decrease in overall stability increases the chance of a column density being momentarily sent

to an artificially low value. When this happens, because that line may become very weak, its Hessian components corresponding to its redshift also become small, and its parameter update can become large. This means it can (mistakenly) be moved far from its current (appropriate) position to some arbitrary (inappropriate) position. Since this is hard to recover from, an easy solution is to temporarily fix all absorption line redshifts, whilst the secondary species column densities ‘recover’ from default-initialisation values to near-optimal values.

4. After minimising χ^2 to refine all free parameters above, the fourth action taken at this Stage is to remove the temporary parameter holds described above and again to minimise χ^2 to refine all interesting parameters.

2.6.2 Refining

5. Interlopers are introduced to the model in Stage 3. If the spectral dataset comprises multiple segments (i.e. several transitions from several different atomic species), one trial interloper is added to every segment simultaneously, the parameters are refined, and interlopers are kept if the *overall* AICc decreases; in fact, an interloper might increase the *local* AICc (i.e. for the spectral segment it lies in). For computational efficiency, to ensure that spurious interlopers do not remain in the model, this is dealt with in Stage 5 by removing each interloper one at a time and only retaining each if the overall AICc does not increase.

6. It is possible that at this Stage of the whole process that the model contains regions where too many heavy element parameters have been introduced, i.e. over-fitting has occurred. There are several ways in which over-fitting could occur for the heavy element lines: (i) In Stage 1, the primary model is developed. In Stage 2, the velocity structure from the primary species is replicated to ensure that any velocity components present in the primary species are also present in the secondary species. However, local least-squares fitting in VPFIT could result in one of the secondary species’ components falling below a threshold and being rejected from the model. This problem is remedied in the ‘Preparation’ step above, in order to keep the model ‘physical’. Thus, the replacement of secondary species components is based purely on physical grounds and not on statistical grounds, i.e. in fact the replacement could produce a *higher* value of AICc, but this is not considered. For this reason, the replacement just described (i.e. requiring all velocity components to be present in all species), creates a marginal tendency to overfit the data. (ii) Another potential way in which slight overfitting can be created is as follows. In Stage 1, when the primary species model is developed, velocity structure is built up by adding one line at a time. This is done using a Monte Carlo process (i.e. trial lines are placed randomly within the data fitting region, repeating the procedure several times and selecting the best (lowest AICc) solution from the set of trials. Because the number of trials is finite, it is occasionally possible to find a local rather than an absolute AICc minimum when accepting a velocity component. In this sense, the *order* in which velocity components are added into the model can influence the final best-fit primary species model. This provides another mechanism by which spurious components may remain in the best-fit primary species model, which are carried forward to the next Stages.

2.7 Modelling line broadening; temperature fit

If the incorrect broadening model is used to generate the absorption profiles (when fitting multiple atomic species simultaneously), this

can impact adversely on the derived velocity structure. Consider a simple absorption system comprising only MgII2796 and FeII2383 profiles. Suppose the intrinsic gas broadening is thermal but that we use turbulent broadening to model the observed profiles. In this case, the model MgII profile will be slightly too narrow and the model FeII profile will be slightly too broad. Two mechanisms can easily compensate for this: (a) a model with 2 velocity components can match the observed profiles by adjusting the relative column densities accordingly, or (b) an interloper can be blended with the MgII profile and b_{turb} adjusted accordingly to match the data. When α is an additional fitting parameter, the effects just described can add a significant systematic uncertainty.

The discussion above illustrates the importance of using the correct broadening method. The procedure to achieve this is:

- (i) Where applicable (i.e. where different atomic species with sufficiently different atomic masses are present) the b -parameters are changed such that they are related (tied) by $b^2 = b_{turb}^2 + b_{th}^2$, where $b_{th}^2 = 2kT/m$, m is atomic mass, and T is the gas temperature. Clearly this requires a new free parameter, T , for each velocity component in the absorption complex.
- (ii) The temperature parameter T can be included, if appropriate, at the beginning of Stage 2.

3 TESTING AI-VPFIT WITH SYNTHETIC SPECTRA

A fully automated modelling process such as the one described in this paper opens new opportunities to scrutinise the limitations present in previous analyses. In particular, we do not know *a priori* whether the broadening of any particular absorption component is purely thermal, purely turbulent, or a hybrid. Many earlier analyses of quasar absorption systems assumed the broadening mechanism from the outset (usually assumed to be turbulent) and constructed models based on that assumption. The justification for doing so was that the assumption should not bias the measured $\Delta\alpha/\alpha$ one way or the other. Whilst this is true, an important point has been overlooked; fitting the wrong model inevitably not only leads to incorrect velocity structure, but importantly, produces systematically over-fitted models. This has important and very undesirable consequences, as we now demonstrate using synthetic spectra.

3.1 Generating synthetic spectra

We base synthetic spectra on the $z_{abs} = 1.15$ absorption complex in the spectrum of the bright quasar HE 0515-0414. The choice is unimportant and some other system could equally have been used. This particular absorption complex spans an unusually large redshift range, $1.14688 < z_{abs} < 1.15176$, corresponding to a velocity range ~ 700 km/s. It is not necessary to use such an extensive range for the purposes required here. We therefore use a subset of the system spanning the redshift range $1.14688 < z_{abs} < 1.14742$, corresponding to a velocity range ~ 100 km/s. For simplicity we simulate only three transitions, Mg II 2796 and 2803 Å and Fe II 2383 Å.

The simulated spectra are Voigt profiles convolved with a Gaussian instrumental profile with $\sigma_{res} = 1.11$ km/s. The pixel size is approximately 0.83 km/s and the signal to noise ratio per pixel is 100 (the noise is taken to be Gaussian). The resolution and pixel size correspond to those of the HARPS instrument on the ESO 3.6m telescope. We derive the input absorption line parameters as follows. In the redshift range $1.14688 < z_{abs} < 1.14742$,

using AI-VPFIT to analyse existing HARPS spectra, we find a total of eight heavy element absorption components plus one interloper. We model the (real) data including a temperature parameter for each absorption component in the complex i.e. each component has both a turbulent and a thermal component to its observed b -parameter. This AI-VPFIT model becomes one of the synthetic models. We call this the “*temperature*” model. The detailed parameters used to create the *temperature* synthetic spectrum are given in Table 1.

3.2 AI-VPFIT models at each Stage

Fig. 1 illustrates the evolution of the model at various points during Stage 1. Each panel shows a different generation. The initial (Scratch) model is a single randomly-placed line. At the end of Stage 1, the line has broadened and the column density increased to minimise χ^2 . The subsequent generations show how the model gradually evolves as more components are added. Only the primary species is shown (MgII in this case), as secondary species are not yet included. By generation 10, the model is already good, although no interlopers have been considered so the feature at ~ -60 km/s is (incorrectly, but knowingly) modelled as MgII. This problem is caught at Stage 3. In the example shown, AI-VPFIT continued iterating up to generation 29 but (on the basis of AICc), decided no additional velocity components were required, i.e. the model did not change for the last 19 generations.

Fig. 2 shows the development of the model through each Stage. For Stages 1 through 5, the model illustrated is from the end of those stages. In the example used, generation 10 is the end-point of Stage 1 so is replicated as the top-left panel in Fig. 2. The model at the end of Stage 1 comprises 10 components. In Stage 2, the secondary species (in this case only FeII) is included. The panel illustrating Stage 6 shows the initial condition of that Stage, where all primary species’ velocity components present by the end of Stage 5 are included but *all* corresponding secondary species components are *replaced*. In the example used, 3 weak FeII components (at about -60 , $+35$, and $+90$ km/s) are replaced as the initial condition for Stage 6. The motivation for doing so is to check that a genuine heavy element velocity component in the secondary species has not been mistakenly replaced by an interloper in Stage 5 (this is possible since the decision making is based purely on AICc).

The final best-fit velocity structure is virtually indistinguishable from true model, labelled (“Fiducial”) and highlighted with a red box to indicate this is the input and not a fitted model: the number of derived absorption components is 8 with one interloper in the MgII2796 line.

4 THE IMPORTANCE OF THE FREE PARAMETER T

The decision as to which type of absorption line broadening to use when fitting real data is important. As alluded to earlier, previous analyses have generally assumed turbulent broadening on the basis that the assumption cannot bias estimating $\Delta\alpha/\alpha$. This assumption seems reasonable intuitively and is likely to be correct in a statistical sense. However, in fact it turns out that the choice of line broadening in the modelling procedure is very important.

In Section 3, AI-VPFIT was applied to a synthetic spectrum generated with *temperature* broadening. This is of course not the only option. Most modelling of high resolution quasar spectra has previously been carried out assuming either *turbulent* or *thermal*

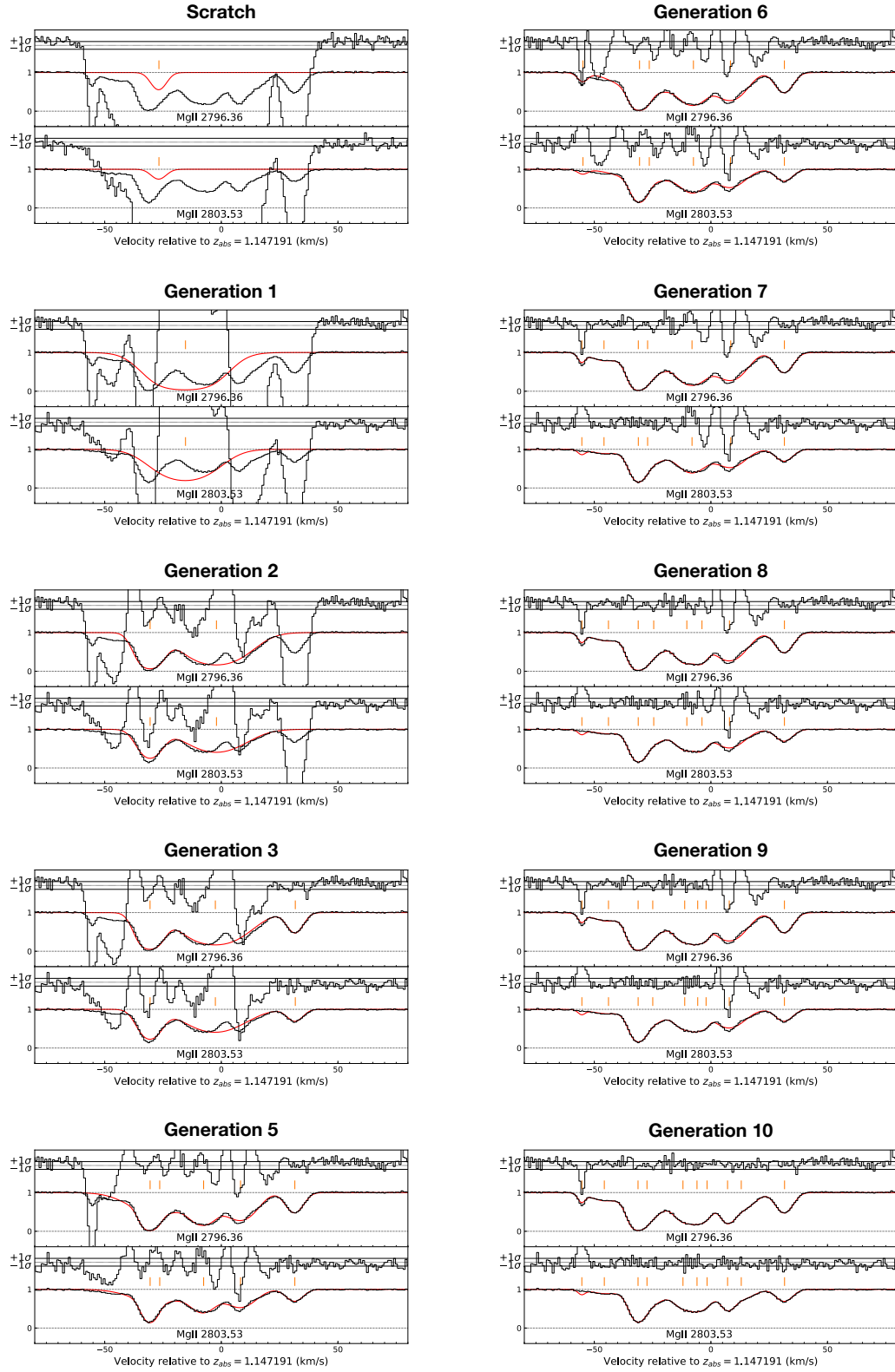


Figure 1. Model evolution through Stage 1 of the AI-VPFIT process. The black histogram illustrates the synthetic *temperature* spectrum. The signal-to-noise per pixel is 100. The continuous red line in the panel labelled “Scratch” shows the initial condition i.e. the randomly placed first-guess line. No VPFIT generation has taken place. The continuous red line in subsequent panels (i.e. “Generation #”) shows the best-fit *temperature* model after each generation of VPFIT. The $\pm 1\sigma$ normalised residuals are plotted at the top of each panel.

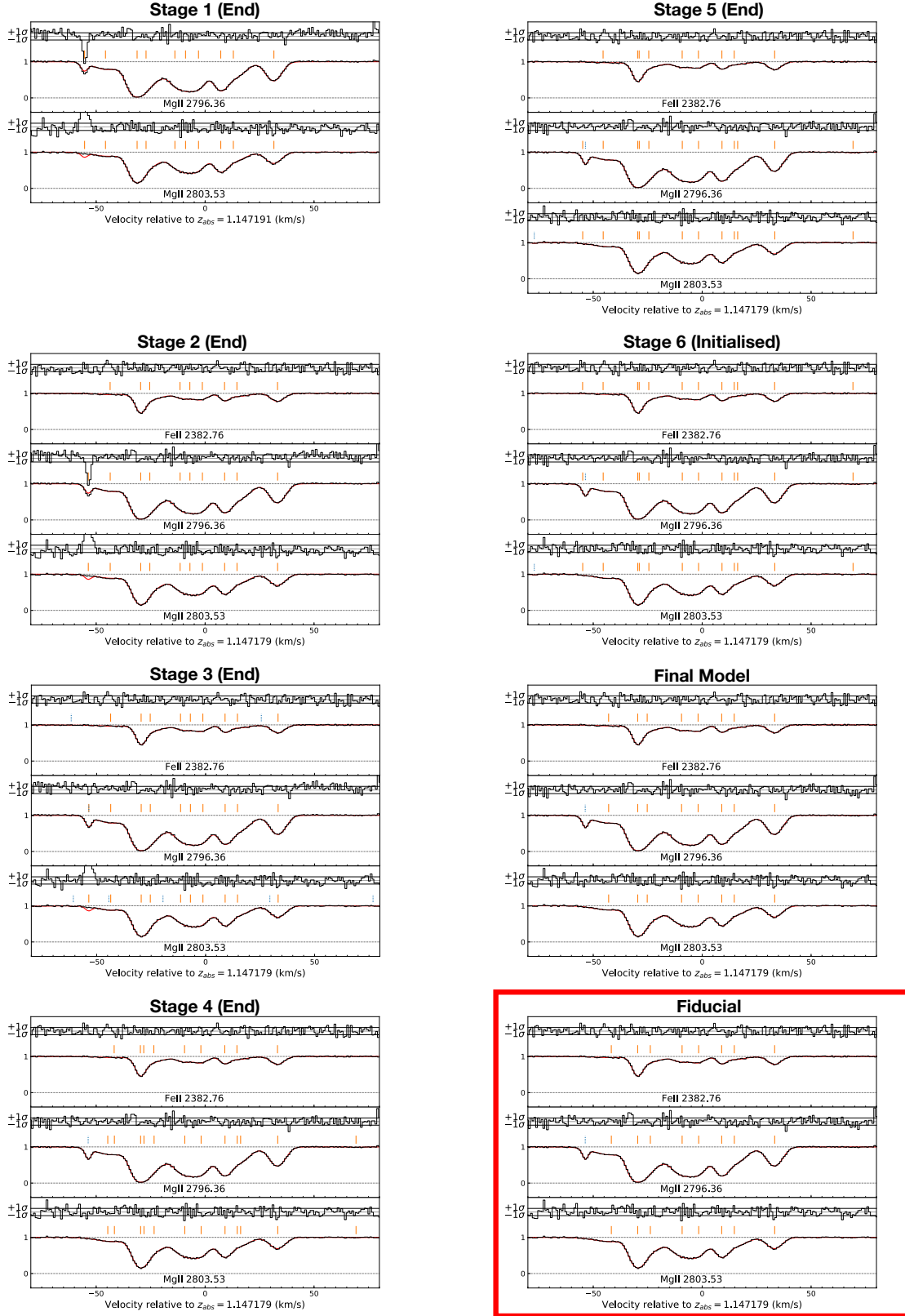


Figure 2. Model evolution at each Stage in AI-VPFIT. The black histogram shows the synthetic spectrum (temperature line broadening). The signal-to-noise per pixel is 100. The red continuous line illustrates the best-fit *temperature* model. For Stages 1 through 5, the end-model is shown. For Stage 6, we illustrate the model at the commencement of the stage, to show how the current velocity structure of the primary species (Mg in this case) is re-introduced to the secondary species (FeII), for the reasons explained in Section 2.6.

No.	log N (MgII)	log N (FeII)	Redshift	Temperature				Turbulent	Thermal	
				b_{turb}	T/K	$b_{\text{th}}(\text{Mg})$	$b_{\text{th}}(\text{Fe})$	$b(\text{Mg}) = b(\text{Fe})$	$b(\text{Mg})$	$b(\text{Fe})$
1	12.03	11.34	1.1468830	8.37	6.52E+04	6.68	4.41	10.71	10.71	7.07
2	12.76	12.33	1.1469678	1.67	1.82E+04	3.53	2.33	3.90	3.90	2.57
3	12.31	11.91	1.1470124	5.43	0.00E+00	0.00	0.00	5.43	5.43	3.58
4	12.59	11.92	1.1471152	4.35	3.81E+04	5.11	3.37	6.71	6.71	4.43
5	12.36	11.77	1.1471692	2.86	2.39E+04	4.04	2.67	4.95	4.95	3.27
6	12.35	11.74	1.1472435	0.80	1.85E+04	3.56	2.35	3.65	3.65	2.41
7	12.17	11.68	1.1472894	5.73	1.19E+04	2.85	1.88	6.40	6.40	4.23
8	12.15	11.97	1.1474175	3.58	1.11E+04	2.76	1.82	4.52	4.52	2.98
Interloper	log N		Redshift	b						
1	12.00		3.9381818	0.80						

Table 1. Model parameters used to generate the three synthetic spectra discussed in Sections 3 and 4. The model comprises eight heavy element components and one interloper. Columns 5-8 correspond to the *temperature* synthetic spectrum, column 9 to the *turbulent* one, and columns 10, 11 to the thermal one. Columns 7 and 8 are the thermal b -parameters for MgII and FeII, i.e. $\sqrt{2kT/m(\text{Mg}, \text{Fe})}$. MgII and FeII have the same b -parameter for turbulent broadening, as shown in column 9. Columns 10 and 11 give the thermal b -parameters for MgII and FeII with $b(\text{FeII}) = b(\text{MgII})\sqrt{m(\text{Mg})/m(\text{Fe})}$. All b -parameters have units of km/s.

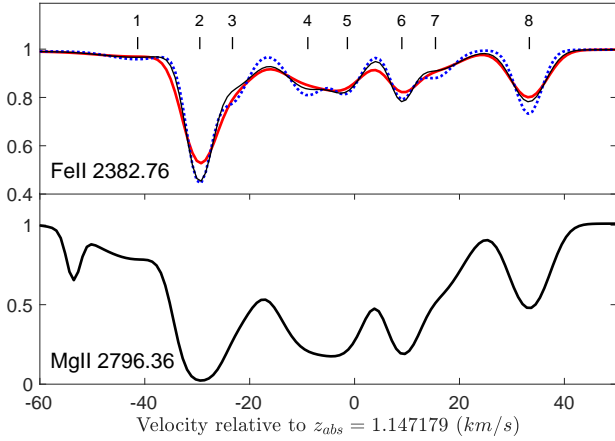


Figure 3. Upper panel: FeII 2383 for *turbulent* (red continuous curve), *thermal* (blue dotted curve) and *temperature* (thin black curve) broadening. Lower panel: MgII 2786, where the line broadening is $b_{\text{th}}(\text{Mg})$ from Table 1. The figure illustrates the variations between each broadening model and hence highlights the importance of using the correct fitting model. For example, line 2 has a low turbulent b -parameter and a relatively high temperature, so the thermal and temperature line centres are similar and much deeper than the turbulent line. Line 8 has a larger turbulent b -parameter and a lower temperature, so the turbulent and temperature models are closer, the deeper line centre being the thermal model.

broadening or both. Here we show the pitfalls of these assumptions and argue that, for reliable results, it is important to include an additional free parameter, T , for each velocity component in the model.

We begin by generating 2 additional synthetic spectra; to create the *turbulent* synthetic model, all parameters are kept the same except for the b -parameter of each absorption component, which is now set to be equal to the Mg II turbulent component. To create the *thermal* synthetic model, we again use the observed MgII b -parameters, although now the FeII b -parameters are adjusted according to their atomic mass. The result of the above is the creation of 3 synthetic spectra, one where the line broadening takes into account both turbulent and thermal components of the b -parameter, one where the broadening is assumed to be purely turbulent, and one where the broadening is assumed to be purely thermal. The

detailed parameters used to create the *turbulent* and *thermal* synthetic spectra are given in Table 1. Those model spectra (and the corresponding *temperature* model), are as shown in Fig. 3.

Fig. 4 shows a set of nine results. Each of the three synthetic spectra (*turbulent*, *thermal*, and *temperature* line broadening) was modelled assuming each line broadening mechanism. The spectrum and model in each panel is as described in the figure caption. The continuous orange vertical lines and blue dashed lines indicate the line centres of the heavy element and interlopers absorption components. Figs. 5, 6, and 7 present the central values and errors for the log N , z and b -parameters from each best-fit model in Fig. 4. These figures illustrate that modelling a *turbulent* spectrum with a *thermal* model leads to errors, and *vice versa*. AI-VPFIT sometimes needs two components to achieve the best-fit model for what is in reality a single component. The parameter error estimates are typically poorly determined for these “double components”.

Whilst ensuring that the model solves simultaneously for both thermal and turbulent components of the observed b -parameter, this does come with a cost, and may not always be possible. If the species fitted simultaneously (i.e. the primary and secondary species) have fairly similar atomic masses, b_{turb} and b_{th} approach degeneracy, leading to a huge uncertainty estimates on the gas temperature. In the synthetic models explored here, the only two elements “observed” are Mg ($A=24$) and Fe ($A=56$). Even then, slight degeneracy translates into quite large uncertainties, as is illustrated in the bottom right panel in Figs. 5, 6, and 7.

Table 2 summarises the results discussed above. When the synthetic spectrum broadening and fitted model broadening match, we can see that the number of absorption components needed to satisfactorily fit the data is minimised (top black line in each section in the table). Conversely, when the “wrong” model is used, additional components are needed. It is now well-established that the line broadening mechanism seen in quasar absorption systems is generally (perhaps never) entirely turbulent or entirely thermal i.e. it is important to use a temperature model. Importantly, for all three synthetic spectra, a temperature model performs very well in terms of finding the correct number of components (last column), as would be expected.

Fig. 8 illustrates the results obtained from modelling the synthetic spectra described above. The figure is divided into three panels, corresponding (top to bottom) to the synthetic data being *turbulent*, *thermal*, and *temperature* respectively. Four $\Delta\alpha/\alpha$ measure-

Spectrum	Model	$\Delta\alpha/\alpha$	$\sigma(\Delta\alpha/\alpha)$	# of lines
<i>Turbulent</i>	<i>Turb</i> (vp)	1.99E-06	2.89E-06	8 + 1
	<i>Turb</i>	2.00E-06	2.56E-06	10 + 2
	<i>Therm</i>	3.42E-06	1.25E-05	13 + 2
	<i>Temp</i>	5.40E-06	3.60E-06	8 + 2
<i>Thermal</i>	<i>Therm</i> (vp)	9.23E-06	3.69E-06	8 + 1
	<i>Turb</i>	-2.86E-07	1.43E-05	11 + 3
	<i>Therm</i>	9.25E-06	3.61E-06	9 + 2
	<i>Temp</i>	1.03E-05	4.05E-06	9 + 1
<i>Temperature</i>	<i>Temp</i> (vp)	1.17E-06	2.66E-06	8 + 1
	<i>Turb</i>	1.42E-05	9.94E-06	11 + 4
	<i>Therm</i>	1.34E-05	4.23E-06	16 + 2
	<i>Temp</i>	1.08E-06	2.50E-06	8 + 1

Table 2. The fitted $\Delta\alpha/\alpha$ for each permutation of synthetic spectrum and model type - illustrated graphically in Fig.8. See the caption to that figure for further details. The last column shows the numbers of heavy element velocity components plus the number of interlopers in the model, within the velocity range of ± 80 km/s, as illustrated in Fig.4.

ments are illustrated within each panel. The highest point illustrates the fitted value of $\Delta\alpha/\alpha$ using VPFIT only, where the starting parameter guesses were the input parameters i.e. the parameters used to generate the synthetic spectrum. The second point down illustrates the result of AI-VPFIT fitting the synthetic data using a *turbulent* model. The third point down illustrates a *thermal* model and the lowest point a *temperature* model. The numerical results are listed in Table 2. The results can be summarised as follows:

- (i) When fitting the synthetic data with the correct model, the results are well-behaved. As expected, the fitted $\Delta\alpha/\alpha$ agrees well with the true value (illustrated by the vertical dashed line in Fig.8).
- (ii) When the *wrong* model is used, the $\Delta\alpha/\alpha$ uncertainty estimate is magnified by a factor of 3 or 4. This is because imposing the wrong broadening mechanism necessarily results in additional velocity components (heavy elements or interlopers or both) being introduced to achieve a satisfactory fit to the data. The consequence of the additional fitting parameters is that $\Delta\alpha/\alpha$ is more poorly constrained. In the last case (*temperature* synthetic data), the thermal model produces a $\Delta\alpha/\alpha$ estimate that is almost 2σ away from the correct value.
- (iii) For all three synthetic spectra, when a *temperature* model is used, the results are good, as would be expected, since the model incorporates the full range of possibilities.

The important conclusion of the above that using the wrong broadening mechanism has highly undesirable consequences. The solution is that wherever possible (i.e. when different species with sufficiently different atomic masses are modelled simultaneously), one should use a *temperature* model.

5 MODEL NON-UNIQUENESS AND IMPACT ON $\Delta\alpha/\alpha$

It is important to understand that the modelling process outlined in this paper, in the context of solving for $\Delta\alpha/\alpha$, is *not* the same as the interactive process followed by a human being. In previous studies, where no AI methodology has been used, and where a human has interactively constructed an absorption line model, this is done by assuming throughout that $\Delta\alpha/\alpha = 0$. Once a good model has been found, the procedure generally adopted in previous analyses has been to only then include $\Delta\alpha/\alpha$ as a free parameter.

We show in this Section that in fact very good models can be (and are) found with disparate values of $\Delta\alpha/\alpha$. Given enough computations, different starting points (equivalent to using different random seeds in the AI-VPFIT code) may reach different solutions. Whilst this is a well-known characteristic of non-linear least-squares procedures applied to complex datasets, it has not been studied in any detail in the context of modelling high-resolution quasar absorption spectra.

Fig.9 shows an AI-VPFIT model, obtained using the *thermal* synthetic spectrum fitted using a *turbulent* model. The model illustrated gives good normalised residuals and appears to be a good representation of the data. However, the synthetic spectrum was generated using $\Delta\alpha/\alpha = 5 \times 10^{-6}$, yet the best-fit value found for this particular turbulent fit is $\Delta\alpha/\alpha = 68 \pm 16 \times 10^{-6}$. The model is thus 4σ away from the “true” value in this case. Inspecting the model details reveals how this occurs. Referring to Fig.9, the FeII column density of velocity component AI has decreased relative to its “true” value, to permit the interloper 24. The same effect occurs at velocity component AE. The interloper 25 is actually present in the data. The strong line under the AM and AA components is actually a single component. However, AI-VPFIT has introduced two components here, such that the column densities of the FeII AA and MgII AM component dominate the line centroid positions. The “true” model in fact comprises 8 heavy element velocity components and one interloper (25). However, Fig.9 comprises 10 heavy element components and 5 interlopers.

In this example, clearly a false minimum in χ^2 has been found. There is no *a priori* reason to reject this model. The only potentially tell-tale signs of there being a problem with this model are (i) an apparent excess of close blends (both heavy element-heavy element and heavy element-interloper) in the stronger components, and (ii) the value of $\Delta\alpha/\alpha$ obtained is inconsistent with that obtained using the *turbulent* and *thermal* models Fig.4.

The effect described above, i.e. finding a statistically acceptable model associated with a false minimum, is a natural consequence of an unbiased modelling the process. (An interactive i.e. human method may artificially avoid the problem by fixing $\Delta\alpha/\alpha = 0$ throughout the model-building process). The correct solution is to repeat the whole fitting process at least twice (and preferably more), searching for additional solutions with fewer velocity components and a lower AICc. We also note that, from calculations done so far, the number of acceptable models (i.e. the degree of non-uniqueness) is likely to be reduced when fitting a temperature model (as would be expected).

6 OVERFITTING - AIC AND BIC

In Bainbridge & Webb (2017a,b) and in the present paper we have made extensive use of the AICc statistic (Hurvich & Tsai 1989) to select candidate models. In the course of this work, we also compared AICc results with those using the Bayesian Information Criterion, BIC (Bozdogan 1987). Both statistics add a penalty to the usual χ^2 statistic, the value of which increases with increasing number of model parameters. The purpose is to end up with a final model having the “right” number of parameters. In other words, both AICc and BIC try to limit the model complexity to avoid “over-fitting”. The AICc (Eq.(1)) and BIC penalties are

$$2nk/(n - k - 1) \text{ and } k \log n, \quad (4)$$

where n , k are the number of data points and free parameters respectively.

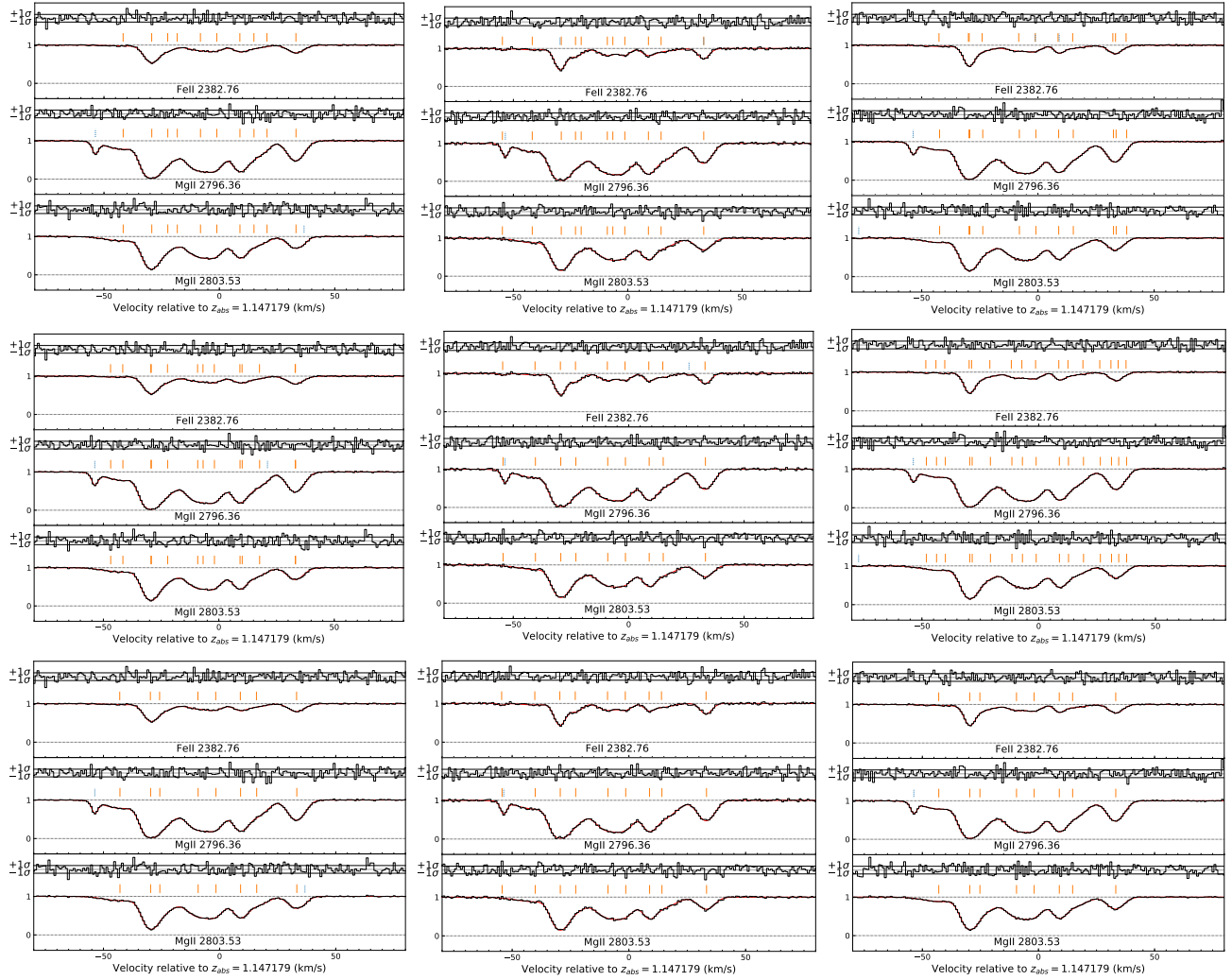


Figure 4. Synthetic spectra and lowest AICc AI-VPFIT models. Tick marks indicate component positions. The signal to noise per pixel is 100. Other parameters used to generate the synthetic spectra are given in Section 3. The left hand column is for the *turbulent* synthetic spectrum, modelled using turbulent broadening (top), thermal broadening (middle), and temperature broadening (bottom). The middle column illustrates the *thermal* synthetic spectrum. The right hand column illustrates the *temperature* synthetic spectrum. Normalised residuals are plotted above each spectrum. The horizontal parallel lines indicate the 1σ ranges.

Fig. 10 illustrates the contribution to the penalty from each free parameter in the model. Placing the spectral fitting boundaries (i.e. defining n) is to some extent arbitrary. Thus in this application to absorption line spectroscopy, a penalty that is relatively insensitive to n is preferable. However, including pixels far from line centre is required if we want to fit continuum parameters. These two considerations alone show that AICc is preferable to BIC in our application.

Nevertheless, even though we have adopted AICc in this paper, it is not entirely suitable. The spectral fitting boundaries influence the AICc penalty and the former are ill-defined. Moreover, for an unsaturated absorption line (for example), pixels far from the line centre impact little on the line profile whilst the converse is true, yet each pixel across the absorption line or complex carries the same weight in the AICc penalty term. Another way of expressing this is that each parameter can influence specific regions within the dataset (but have little or no impact elsewhere); the parameters describing an absorption component at -50 km/s in Fig. 3, for example, have virtually no influence on the model intensity at $+50$ km/s. The AICc

(and BIC) fail to take such an effect into account. AICc is thus not optimal for absorption line spectroscopy and some other (new) statistic is needed.

Finally, the details of model non-uniqueness (Section 5) are likely to depend on the statistic used i.e. AICc or something else. These considerations are beyond the scope of the present paper and will be addressed in subsequent work.

7 DISCUSSION AND CONCLUSIONS

In this paper we have extended previous work that combined a genetic algorithm with non-linear least-squares to automatically model absorption line data. “Interactive” absorption line fitting is subjective and generally not reproducible. The method presented here brings objectivity and repeatability, important requirements for the increasingly high-quality data from new and forthcoming spectroscopic facilities like ESPRESSO/VLT and HIRES/ELT.

An AI method provides an unbiased estimate of $\Delta\alpha/\alpha$. The

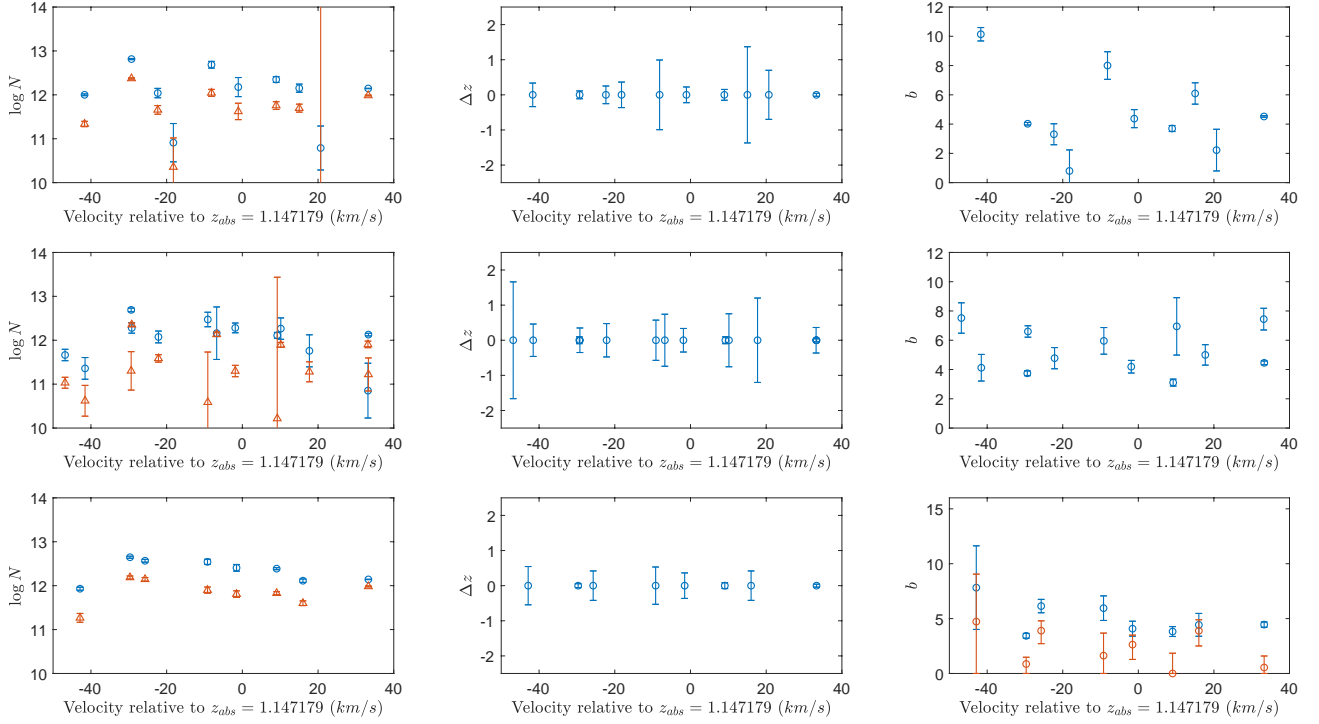


Figure 5. Results of modelling the synthetic *turbulent* spectrum. Top row: the fitted model is a *turbulent* model. Middle row: the fitted model is *thermal*. Bottom row: the fitted model is *temperature*. Blue points (circles) show the best-fit parameters for MgII. Red points (triangles) show the best-fit parameters for FeII. VPFIT error bars for each parameter are shown in all cases. Left: $\log N$ versus velocity. Centre: Redshift uncertainty (from VPFIT) versus velocity. Right: b -parameter versus velocity.

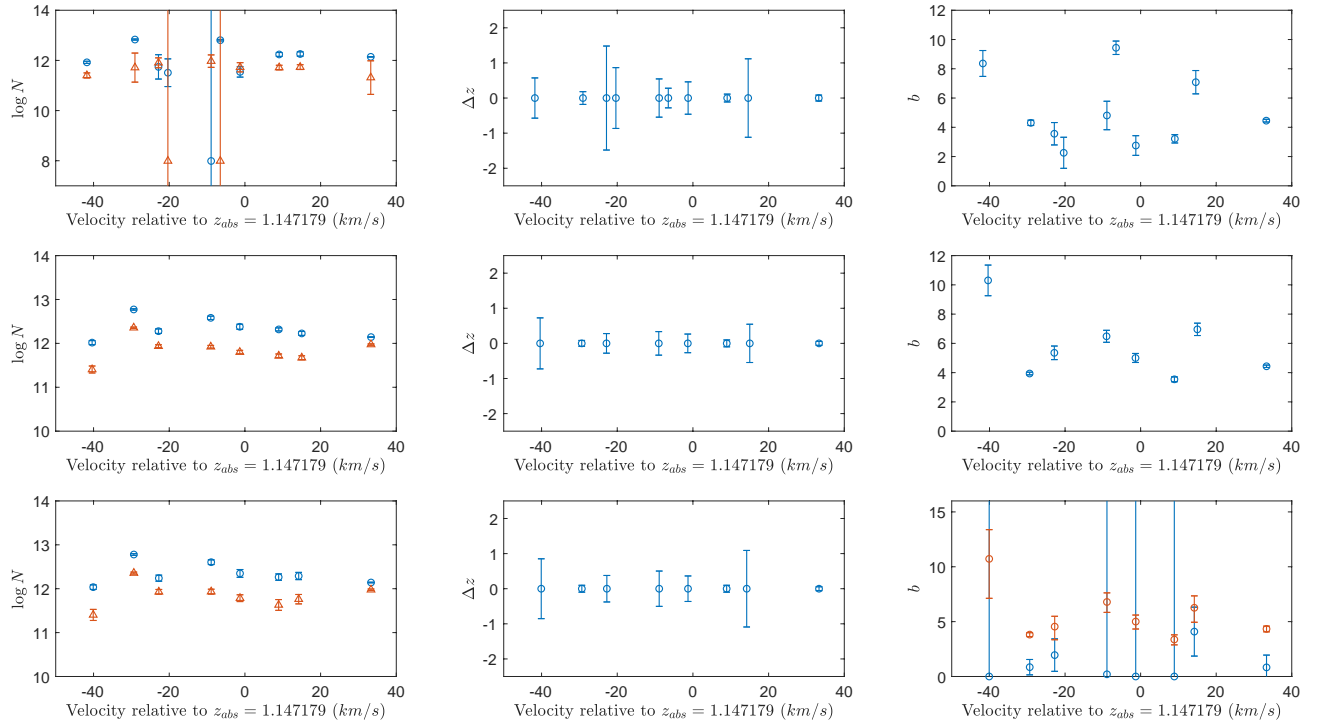


Figure 6. Same as Fig. 5 except using the *thermal* synthetic spectrum.

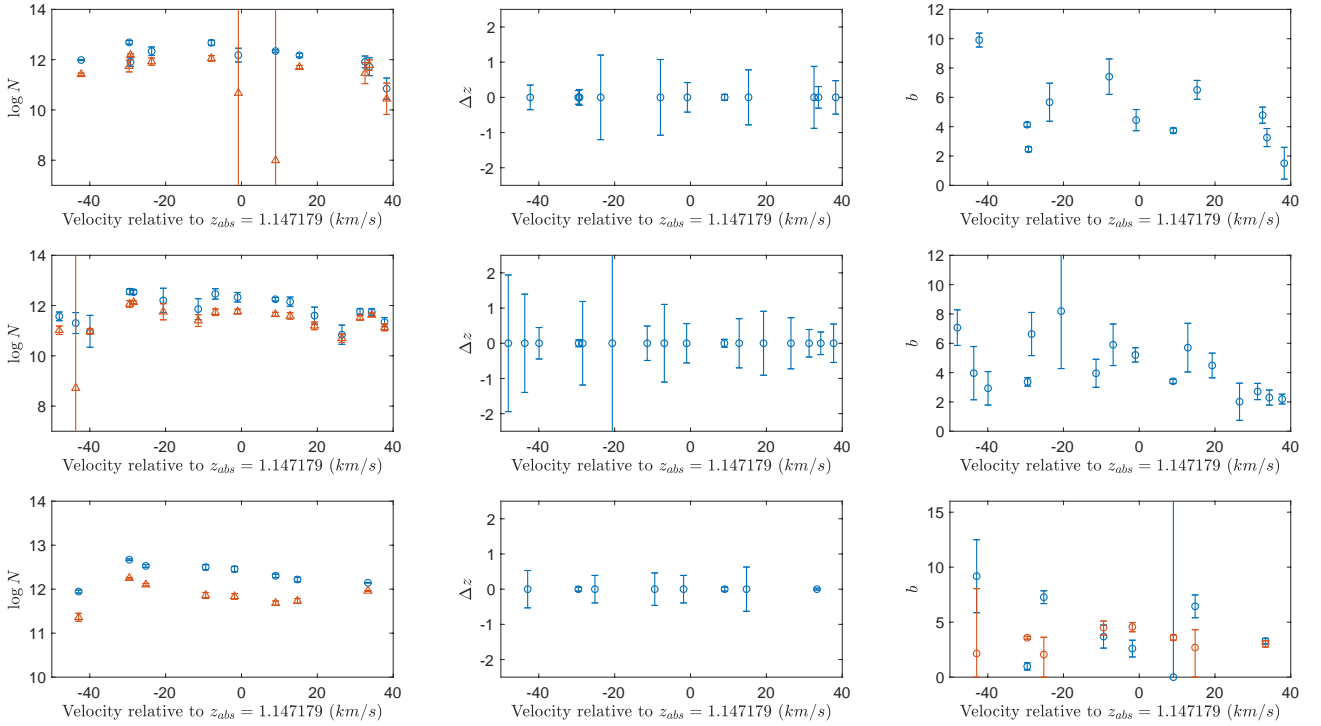


Figure 7. Same as Fig. 5 except using the *temperature* synthetic spectrum.

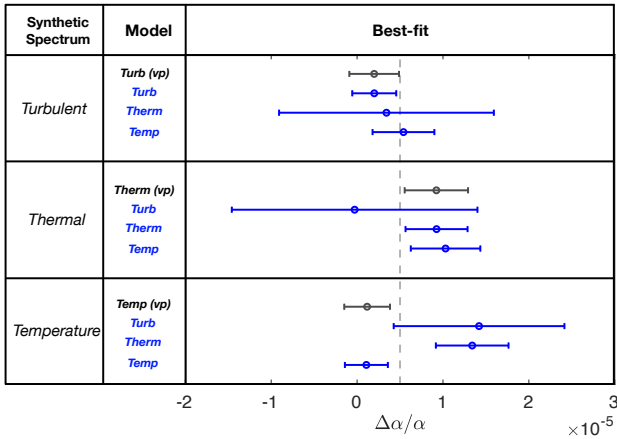


Figure 8. Comparing the fitted $\Delta\alpha/\alpha$ for each permutation of synthetic spectrum and model type. The left-hand column indicates the synthetic spectrum used. The second column indicates the line broadening mechanism used in modelling. “Turb (vp)” means that VPFIT was used with the true model parameters as starting guesses; this point is shown in black in the third column, which also shows the best-fit $\Delta\alpha/\alpha$ for a *turbulent*, *thermal*, and *temperature* model, with corresponding parameter 1σ uncertainties (from VPFIT).

same is not true of any interactive method that holds $\Delta\alpha/\alpha = 0$ during the model construction phase, only to “switch on” $\Delta\alpha/\alpha$ as a free parameter at the end, once the model is essentially complete. A procedure of this sort preferentially selects local minima closest to $\Delta\alpha/\alpha = 0$.

Synthetic spectra, based on a well-known intermediate redshift absorption system, have been created and used to test the method’s

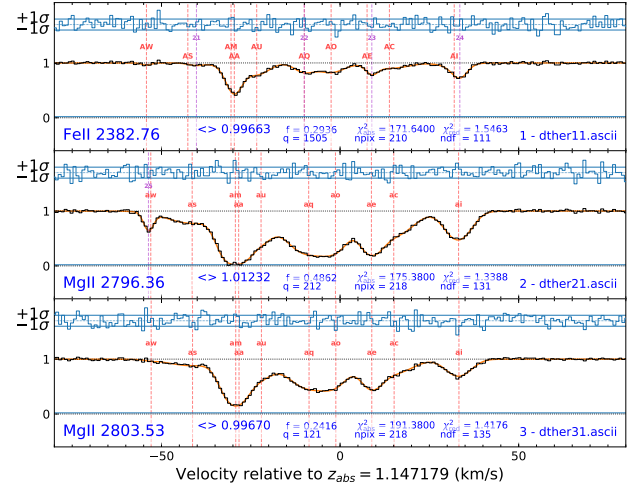


Figure 9. Illustration of the model non-uniqueness problem. The input spectrum is *thermal* and the fitted model is *turbulent*. This model passed all acceptance tests described in Section 2 and is a minimum AICc result with $\chi^2_n = 0.91$. However, it gives $\Delta\alpha/\alpha = 6.78 \pm 1.63 \times 10^{-5}$, compared to the “true” (synthetic spectrum) input value of $\Delta\alpha/\alpha = 5.0 \times 10^{-6}$. The discrepancy is caused by a local χ^2 minimum.

performance. We have shown that model development goes wrong i.e the wrong velocity structure is obtained, if the wrong broadening mechanism is used to model the observational data. High quality observations of quasar absorption systems show that in general the line broadening does indeed contain both thermal and turbulent contributions simultaneously. However, much of the previous work on estimating $\Delta\alpha/\alpha$ has been done assuming a single broadening mechanism. We have shown that there are highly undesirable conse-

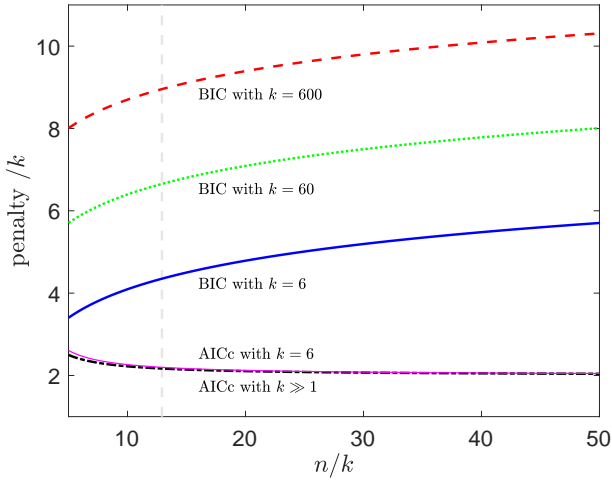


Figure 10. Penalty per free parameter (Eq.4 divided by k) vs. the number of pixels per parameter, n/k . The blue (solid), green (dotted), and red (dashed) curves illustrate the BIC penalty term for different k . At fixed n/k , BIC increases relatively rapidly as more model parameters are introduced. At fixed n/k , BIC also increases as the spectral fitting region n is increased. The magenta (continuous) and black (dot-dash) curves show the AICc penalty term. The AICc penalty is insensitive to k and relatively insensitive to n/k . The vertical grey (dashed) line indicates $n/k = 646/50$ for the synthetic model of Fig.3.

quences of this: the wrong velocity structure may easily be obtained, resulting in far less reliable parameter estimates. Fig. 8 shows this clearly for $\Delta\alpha/\alpha$.

The extent to which this model non-uniqueness issue applies even when the *correct* model is used is not yet clear. It is possible, even likely, that χ^2 -parameter space is sufficiently complex, with multiple local minima, that false minima result even when solving for b_{th} and b_{turb} simultaneously. If so, model non-uniqueness limits the precision achievable from any single measurement i.e. it is not possible to reach the theoretical statistical limit using a single observation of $\Delta\alpha/\alpha$, no matter how precise the wavelength calibration. The implication is that, by nature, the problem of measuring $\Delta\alpha/\alpha$ is a statistical one, requiring a large sample of measurements to render the non-uniqueness systematic negligible. This principle should perhaps underpin all future scientific efforts to determine whether the fine structure constant varies in time or space.

ACKNOWLEDGEMENTS

We are grateful for supercomputer time using OzSTAR at the Centre for Astrophysics and Supercomputing at Swinburne University of Technology. CCL thanks the Royal Society for a Newton International Fellowship during the early stages of this work. JKW thanks the John Templeton Foundation, the Department of Applied Mathematics and Theoretical Physics and the Institute of Astronomy at Cambridge University for hospitality and support, and Clare Hall for a Visiting Fellowship during this work.

REFERENCES

- Bainbridge M. B., Webb J. K., 2017a, *Universe*, **3**, 34
 Bainbridge M. B., Webb J. K., 2017b, *MNRAS*, **468**, 1639
 Bozdogan H., 1987, *Psychometrika*, **52**, 345

- Carswell R. F., Webb J. K., 2014, VPFIT: Voigt profile fitting program, Astrophysics Source Code Library (ascl:1408.015)
 Carswell R. F., Webb J. K., 2020, Bob Carswell’s homepage, <https://people.ast.cam.ac.uk/~rfc/>
 ESO ELT team 2010, The science case for the European Extremely Large Telescope: The next step in mankind’s quest for the Universe. ESO online, https://www.eso.org/sci/facilities/eelt/science/doc/eelt_science_book.pdf
 ESO ELT team 2011, An Expanded View of the Universe Science with the European Extremely Large Telescope. ESO online, https://www.eso.org/sci/facilities/eelt/science/doc/eelt_sciencecase.pdf
 Hook I., 2009, in Moorwood A., ed., Science with the VLT in the ELT Era. Springer Netherlands, Dordrecht, pp 225–232
 Hurvich C. M., Tsai C.-L., 1989, *Biometrika*, **76**, 297
 Liske J., Spyromillio J., Tamai R., 2014, Top Level Requirements for ELT-HIRES, https://www.eso.org/sci/facilities/eelt/docs/ESO-204697_1_Top_Level_Requirements_for_ELT-HIRES.pdf
 Marconi A., et al., 2016, in Ground-based and Airborne Instrumentation for Astronomy VI, eds. Christopher J. Evans and Luc Simard and Hideki Takami. SPIE, pp 676 – 687, doi:10.1117/12.2231653, <https://doi.org/10.1117/12.2231653>
 Moscato P., 1989, On Evolution, Search, Optimization, Genetic Algorithms and Martial Arts - Towards Memetic Algorithms, Technical Report Caltech Concurrent Computation Program, report 826, <http://citeseerx.ist.psu.edu/viewdoc/download?doi=10.1.1.27.9474&rep=rep1&type=pdf>
 Pepe F., et al., 2014, *Astronomische Nachrichten*, **335**, 8

This paper has been typeset from a \LaTeX file prepared by the author.